Research Article | Vol. 27, No. 3 | 4 Feb 2019 | OPTICS EXPRESS 1968
Optics EXPRESS

Analysis and removal of five-dimensional mosaicking errors in mosaic grating

MIN CONG,[1,2] XIANGDONG QI,[1,*] JING XU,[3] CHUAN QIAO,[1,2] XIAOTAO MI,[1] XIAOTIAN LI,[1] HAILI YU,[1] SHANWEN ZHAHNG,[1] HONGZHU YU,[1] AND BAYANHESHIG [1]

[1]*Changchun Institute of Optics, Fine Mechanics and Physics, Chinese Academy of Sciences, Changchun Jilin 130033, China*
[2]*University of Chinese Academy of Science, Beijing 100049, China*
[3]*Deparment of Health Examination Center, The First Hospital of Jinlin University, Changchun Jilin 130021, China*
**chiangrating@263.net*

Abstract: Combining the mathematical relationships between the grating wavefront and surfaces with the spatial relationships between the two grating wavefront, a mathematical model of the mosaicking errors is established to mosaic gratings. The five-dimensional mosaicking errors will respectively be calculated and then removed by the adjustment mechanisms. Mosaicking experiments are performed by using two gratings. First, by using zeroth order, the longitudinal offset is calculated and removed. Second, by using the diffraction order, the in-plane angle and grating spacing are calculated and removed, while the tip and tilt angles are calculated and removed. And then a mosaic grating is obtained.

1. Introduction

In the 1990s, large-scale optical telescopes were built in many locations worldwide. The original monolithic gratings were not large enough for astronomy applications [1], and thus the mosaic grating was proposed [2]. All major telescopes are equipped with a mosaic grating to increase their spectral resolution [3] and satisfy the requirements for astronomical observations. In recent years, the Hobby Eberly Telescope [4], the James Webb Space Telescope [5] and the Thirty Meter Telescope (TMT) [6] have all required some new large-scale mosaic grating for their high-resolution instruments. In other fields, large-scale gratings have been used to increase the damage threshold of laser energies used for inertial confinement fusion (ICF), including OMEGA EP [7–9], PICO2000 [10,11] and FIREX-1 [12]; these systems were all equipped with mosaic gratings.

In 2006, Sauteret [13] discussed the effects of mosaicking errors on a diffraction grating at the focal plane, and a theoretical model of mosaic gratings was established by analysis of the electromagnetic field characteristics on the focal plane. From a three-dimensional perspective, the relationships among the spatio-temporal characteristics of the far-field spot, the spectral profile and the grating mosaic errors were analyzed. In 2006, Zeng et al. [14] proposed a dual-wavelength detection method that introduced two wavelengths of light into the optical path to display the mosaicking errors. However, when the diffraction spots of the two gratings completely overlap and the spot shape satisfies the far-field diffraction theory, large residual mosaicking errors are still present. Then the interferometry is proposed to mosaic gratings. In 2016, Lu et al. [15] proposed the dual-angle incident light method to eliminate the mosaicking errors by using the interference fringes, and they [16] also analyzed the effects of the incident light on the mosaic grating the following year. In 2008, Guardalben [17] analyzed the effects of mosaicking errors on the performance of the mosaic grating by using the rotation matrix method and two-wavelength incident light. All the above methods have been presented how to mosaic gratings and analyzed the effect of the mosaicking errors to the mosaic grating.

#346182 https://doi.org/10.1364/OE.27.001968
Journal © 2019 Received 18 Sep 2018; revised 30 Nov 2018; accepted 30 Nov 2018; published 23 Jan 2019

Optics EXPRESS

However, the values of the mosaicking errors cannot be calculated in the experiment, the mosaicking errors will compensate each other that cannot be detected directly, and the movement data of the adjustment mechanisms cannot be confirmed. So the success of experiment is contingent by using the above methods. In this paper, we will propose an analytical method to manufacture the mosaic grating.

In this paper, a mathematical model of the mosaicking errors is established to manufacture mosaic grating. The Zygo interferometer will detect the wavefront of the two adjacent gratings, and each of the mosaicking errors will be calculated by analyzing the spatial relationships between the fitted planes for the wavefront. According to the calculated values of the mosaicking errors, the compensative effects of the mosaicking errors will be eliminated, and the movement data of the adjustment mechanisms can be confirmed. The mosaicking errors can be analyzed quantitatively and the experiment will be succeeded more effectively. The gratings are mosaicked as per the model, and we finally obtain a mosaic grating.

2. Theory model for mosaic grating

There are six coordinate frames used in the mosaicking error algorithm. Then (x, y, z) is the coordinate frame for the grating surface, (x_1, y_1, z_1) is for the grating G1, and (x_2, y_2, z_2) is for the grating G2. And (u, v, w) is the coordinate frame for the detector that means the diffraction wavefront, (u_1, v_1, w_1) is for the G1 wavefront, and (u_2, v_2, w_2) is for the grating G2 wavefront. The relationships among them are used to calculate the mosaicking errors.

Figure 1 shows the grating coordinate setup, where G1 is the reference grating and G2 is the moving grating. The x-axis is along the indexing direction, the y-axis is along the groove direction, the z-axis is perpendicular to the grating surface. The origin of the coordinate system (x, y, z) is the lower right corner of the reference grating surface. The origin of the coordinate system (x_1, y_1, z_1), where G1 is located, is the center point on the G1's surface. And the origin of the coordinate system (x_2, y_2, z_2), where G2 is located, is the center point on the G2's surface. The angle errors and displacement errors, which are between coordinate system (x_2, y_2, z_2) and coordinate system (x_1, y_1, z_1), are the mosaicking errors. And as shown in Fig. 1 the studies concerns about the flat gratings.

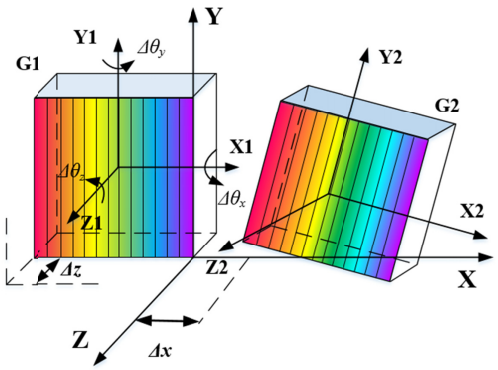

Fig. 1. Mosaicking errors of two adjacent gratings.

There are five-dimensional mosaicking errors. The tip angle is the rotation around the x_1-axis, and is designated $\Delta\theta_x$; the tilt angle is the rotation around the y_1-axis, and is designated $\Delta\theta_y$; the in-plane angle is the rotation around the z_1-axis, and is designated $\Delta\theta_z$; the grating space is the distance between the two gratings along the x_1-axis, and is designated Δx; and the longitudinal offset is the distance between the two gratings along the z_1-axis, and is designated Δz.

The three-dimensional numerical matrices for the two gratings, which contain all the coordinate points of the two grating surfaces, are shown as the Eqs. (1) and (2).

Optics EXPRESS

$$G_1 = \begin{bmatrix} x_{11} & y_{11} & z_{11} \\ x_{12} & y_{12} & z_{12} \\ \vdots & \vdots & \vdots \\ x_{1n} & y_{1n} & z_{1n} \end{bmatrix}. \tag{1}$$

$$G_2 = \begin{bmatrix} x_{21} & y_{21} & z_{21} \\ x_{22} & y_{22} & z_{22} \\ \vdots & \vdots & \vdots \\ x_{2n} & y_{2n} & z_{2n} \end{bmatrix}. \tag{2}$$

Where n is the total number of the points on the grating surface. Because the two gratings are both replicas from a single master for the same generation, the surfaces of the two gratings can be considered to be the same. And the corresponding points between the two gratings are mathematical related as shown in the Eq. (3).

$$G_{2i}{}^T = R_z(\Delta\theta_z)\cdot R_y(\Delta\theta_y)\cdot R_x(\Delta\theta_x)\cdot\left\{G_{1i}{}^T + \begin{bmatrix} \Delta x + L \\ 0 \\ \Delta z \end{bmatrix}\right\}. \tag{3}$$

Here, L is the length of the grating along the indexing direction, X^T means the transposed matrix of X. G_{2i} is any point on the grating G2 and G_{1i} is that for the grating G1 as shown in Eq. (4).

$$\begin{cases} G_{1i} = [x_{1i},\ y_{1i},\ z_{1i}] \\ G_{2i} = [x_{2i},\ y_{2i},\ z_{2i}] \end{cases}. \tag{4}$$

And $R_x(\theta)$, $R_y(\theta)$ and $R_z(\theta)$ are the rotation matrices around the x_1-axis, the y_1-axis and the z_1-axis, expressed as shown in the Eq. (5), respectively.

$$\begin{aligned} R_x(\theta) &= \begin{bmatrix} 1 & 0 & 0 \\ 0 & \cos\theta & \sin\theta \\ 0 & -\sin\theta & \cos\theta \end{bmatrix}, \\ R_y(\theta) &= \begin{bmatrix} \cos\theta & 0 & -\sin\theta \\ 0 & 1 & 0 \\ \sin\theta & 0 & \cos\theta \end{bmatrix}, \\ R_z(\theta) &= \begin{bmatrix} \cos\theta & \sin\theta & 0 \\ -\sin\theta & \cos\theta & 0 \\ 0 & 0 & 1 \end{bmatrix}. \end{aligned} \tag{5}$$

The Zygo interferometer can detect the wavefront of the two adjacent gratings after coarse adjustment, where the two far-field spots of the two adjacent gratings should be overlap to ensure that the interference fringes of the two gratings can be detected simultaneously. Then, the three-dimensional numerical matrices for the wavefront are shown as the Eqs. (6) and (7) below, which are measured by the Zygo interferometer.

$$\Delta_1 = \begin{bmatrix} u_{11} & v_{11} & w_{11} \\ u_{12} & v_{12} & w_{12} \\ \vdots & \vdots & \vdots \\ u_{1n} & v_{1n} & w_{1n} \end{bmatrix}. \tag{6}$$

Optics EXPRESS

$$\Delta_2 = \begin{bmatrix} u_{21} & v_{21} & w_{21} \\ u_{22} & v_{22} & w_{22} \\ \vdots & \vdots & \vdots \\ u_{2n} & v_{2n} & w_{2n} \end{bmatrix}. \tag{7}$$

Here, and n is the total number of the points for the wavefront. u and v are the pixels that correspond to the detector locations, the measurement accuracy of them is 1pixel. And w represents the wavefront of the grating, the measurement accuracy can reach 10^{-10} μm [18,19]. Δ_1(m) is the numerical matrix for the wavefront refers to G1 and Δ_2(m) is that refers to G2. The corresponding points between the grating surface and the wavefront on the detector are mathematical related as follows:

$$\begin{cases} \Delta_{1i}{}^T = \left[R_y(\theta_i) + R_y(\theta_k) \right] \cdot G_{1i}{}^T \\ \Delta_{2i}{}^T = \left[R_y(\theta_i) + R_y(\theta_k) \right] \cdot G_{2i}{}^T \end{cases}. \tag{8}$$

Here, θ_i is the incidence angle, and θ_k is the diffraction angle, Δ_{1i} and Δ_{2i} are the corresponding points on the detector as shown in Eq. (9).

$$\begin{cases} \Delta_{1i} = \left[u_{1i}, \quad v_{1i}, \quad w_{1i} \right] \\ \Delta_{2i} = \left[u_{2i}, \quad v_{2i}, \quad w_{2i} \right] \end{cases}. \tag{9}$$

Because of the mosaicking errors, the wavefront of the two gratings will be different which will be shown on the interference fringes, such as different slope or different periods. And after the coarse adjustment, the mosaicking errors are small quantities which are less than 100μrad and 2μm.

Thus, solve the Eqs. (3) and (8), and using the grating equation Eq. (10) and the principle which the small first-order quantity is retained while the second-order or smaller quantities can be ignored, the relationship between the grating surface and the wavefront can be obtained as the Eqs. (11) and (12).

$$d \cdot \left(\sin\theta_i + \sin\theta_k \right) = m \cdot \lambda. \tag{10}$$

Here, d is the grating constant, λ is the wavelength of the incident light, and m is the diffraction order.

$$\Delta_{1i}{}^T(m) = \begin{bmatrix} x_{1i} \cdot \left(\cos\theta_i + \cos\theta_k \right) - z_{1i} \cdot \dfrac{m\lambda}{d} \\ 2 \cdot y_{1i} \\ x_{1i} \cdot \dfrac{m\lambda}{d} + z_{1i} \cdot \left(\cos\theta_i + \cos\theta_k \right) \end{bmatrix}. \tag{11}$$

$$\Delta_{2i}{}^T(m) = \begin{bmatrix} \left(x_{1i} + \Delta x + y_{1i} \cdot \Delta\theta_z \right) \cdot \left(\cos\theta_i + \cos\theta_k \right) - \left(z_{1i} + x_{1i} \cdot \Delta\theta_y - y_{1i} \cdot \Delta\theta_x + \Delta z \right) \cdot \dfrac{m\lambda}{d} \\ 2 \cdot \left(y_{1i} - x_{1i} \cdot \Delta\theta_z \right) \\ \left(x_{1i} + \Delta x + y_{1i} \cdot \Delta\theta_z \right) \cdot \dfrac{m\lambda}{d} + \left(z_{1i} + x_{1i} \cdot \Delta\theta_y - y_{1i} \cdot \Delta\theta_x + \Delta z \right) \cdot \left(\cos\theta_i + \cos\theta_k \right) \end{bmatrix}. \tag{12}$$

Based on the measurement accuracy for u, v and w, where the measurement accuracy of u and v is 1pixel, and the measurement accuracy of w is 10^{-10}μm, the Eq. (12) can be simplified as shown below.

Optics EXPRESS

$$\Delta_{2i}{}^{T}(m)=\begin{bmatrix} x_{1i}\cdot(\cos\theta_i+\cos\theta_k)-z_{1i}\cdot\dfrac{m\lambda}{d} \\ 2\cdot y_{1i} \\ (x_{1i}+\Delta x+y_{1i}\cdot\Delta\theta_z)\cdot\dfrac{m\lambda}{d}+(z_{1i}+x_{1i}\cdot\Delta\theta_y-y_{1i}\cdot\Delta\theta_x+\Delta z)\cdot(\cos\theta_i+\cos\theta_k) \end{bmatrix}. \tag{13}$$

The Eqs. (11) and (13) represent the relationship between the grating surface and the wavefront within the mosaicking errors.

If the zeroth order is used, $m = 0$, and then the Eqs. (11) and (13)can be further simplified.

$$\Delta_{1i}{}^{T}(0)=\begin{bmatrix} x_{1i}\cdot(\cos\theta_i+\cos\theta_k) \\ 2\cdot y_{1i} \\ z_{1i}\cdot(\cos\theta_i+\cos\theta_k) \end{bmatrix}. \tag{14}$$

$$\Delta_{2i}{}^{T}(0)=\begin{bmatrix} x_{1i}\cdot(\cos\theta_i+\cos\theta_k) \\ 2\cdot y_{1i} \\ (z_{1i}+x_{1i}\cdot\Delta\theta_y-y_{1i}\cdot\Delta\theta_x+\Delta z)\cdot(\cos\theta_i+\cos\theta_k) \end{bmatrix}. \tag{15}$$

Therefore, Δx and $\Delta\theta_z$ do not affect the zeroth-order wavefront. In accordance with this phenomenon, the mosaicking errors can be removed in two parts. Δz is removed by measuring and analyzing the zeroth-order wavefront, and $\Delta\theta_x$ and $\Delta\theta_y$ are also removed preliminary. $\Delta\theta_z$ and Δx are removed by measuring and analyzing the diffraction-order wavefront, and $\Delta\theta_x$ and $\Delta\theta_y$ are removed again.

According to the numerical matrices for the wavefront, where are the Eqs. (6) and (7), the wavefront will be fitted to the planes by using the least squares principle. The spatial relation of the fitted planes can be calculated, which are the mosaicking errors. And then they will be removed to manufacture the mosaic grating.

The fitted plane for the wavefront is set as follows:

$$w = a\cdot u + b\cdot v + c. \tag{16}$$

Here, a, b and c are constants that represent the plane coefficients. In accordance with the least squares principle, coefficients a, b and c can be determined when the Eqs. (17) and (18) are both satisfied.

$$S=\sum_t\left[w_t-(au_t+bv_t+c)\right]^2. \tag{17}$$

$$\begin{bmatrix} \sum u_t^2 & \sum u_t\cdot v_t & \sum u_t \\ \sum u_t\cdot v_t & \sum v_t^2 & \sum v_i \\ \sum u_t & \sum v_t & \sum 1 \end{bmatrix}\cdot\begin{bmatrix} a \\ b \\ c \end{bmatrix}=\begin{bmatrix} \sum u_t\cdot w_t \\ \sum v_t\cdot w_t \\ \sum w_t \end{bmatrix}. \tag{18}$$

The fitted planes for the wavefront can be obtained according to the Eqs. (6) and (7), and the Eqs. (16) – (18).

The zeroth order is analyzed. Δz are calculated by using the zeroth-order wavefront of the two gratings, while $\Delta\theta_x$ and $\Delta\theta_y$ are calculated.

When $m = 0$, the two fitted planes for the zeroth-order wavefront of the two gratings are shown in the Eq. (19).

$$\begin{cases} w_1 = a_{10}u_1 + b_{10}v_1 + c_{10} \\ w_2 = a_{20}u_2 + b_{20}v_2 + c_{20} \end{cases}. \tag{19}$$

Optics EXPRESS

Take the Eq. (14) to the Eq. (19), the mathematical relationships between the two grating surfaces and the two fitted planes for the zeroth-order wavefront can be obtained as the Eq. (20).

$$\begin{cases} G_1: \left(\cos\theta_i+\cos\theta_k\right)\cdot z_{1i} = a_{10}\left(\cos\theta_i+\cos\theta_k\right)\cdot x_{1i} + 2b_{10}\cdot y_{1i} + c_{10} \\ G_2: \left(\cos\theta_i+\cos\theta_k\right)\cdot z_{2i} = a_{20}\left(\cos\theta_i+\cos\theta_k\right)\cdot x_{2i} + 2b_{20}\cdot y_{2i} + c_{20} \end{cases}. \tag{20}$$

The normal vectors of the two fitted planes for the zeroth-order wavefront of the two gratings are then shown as the Eq. (21) below.

$$\begin{cases} \overrightarrow{n_{g10}} = \left[a_{10}, \quad \dfrac{2b_{10}}{\left(\cos\theta_i+\cos\theta_k\right)}, \quad -1 \right] \\ \overrightarrow{n_{g20}} = \left[a_{20}, \quad \dfrac{2b_{20}}{\left(\cos\theta_i+\cos\theta_k\right)}, \quad -1 \right] \end{cases}. \tag{21}$$

The spatial relationship between the two fitted planes for the zeroth-order wavefront of the two gratings is given as shown in the Eq. (22).

$$\overrightarrow{n_{g10}}^{T} = R_x\left(\Delta\theta_x\right)\cdot R_y\left(\Delta\theta_y\right)\cdot \overrightarrow{n_{g20}}^{T}. \tag{22}$$

Using the Eq. (22), $\Delta\theta_x$ and $\Delta\theta_y$ can be obtained. And Δz can be obtained by using the Eqs. (14), (15) and (20), as shown in the Eq. (24).

$$\Delta z = \frac{c_{10}-c_{20}}{\cos\theta_i+\cos\theta_k}. \tag{23}$$

Then the diffraction order is analyzed. $\Delta\theta_z$ and Δx are calculated using the diffraction-order wavefront of the two gratings, while $\Delta\theta_x$ and $\Delta\theta_y$ are again calculated.

When $m \neq 0$, the two fitted planes for the diffraction-order wavefront of the two gratings are shown in the Eq. (24).

$$\begin{cases} w_1 = a_{1m}u_1 + b_{1m}v_1 + c_{1m} \\ w_2 = a_{2m}u_2 + b_{2m}v_2 + c_{2m} \end{cases}. \tag{24}$$

Take the Eq. (11) to the Eq. (24), the mathematical relationships between the two grating surfaces and the two fitted planes for the diffraction-order wavefront can be obtained as the Eq. (25).

$$\begin{cases} G_1: x_{1i}\cdot\dfrac{m\lambda}{d} + z_{1i}\cdot\left(\cos\theta_i+\cos\theta_k\right) = a_{1m}\cdot\left[x_{1i}\cdot\left(\cos\theta_i+\cos\theta_k\right) - z_{1i}\cdot\dfrac{m\lambda}{d}\right] + 2b_{1m}\cdot y_{1i} + c_{1m} \\ G_2: x_{2i}\cdot\dfrac{m\lambda}{d} + z_{2i}\cdot\left(\cos\theta_i+\cos\theta_k\right) = a_{2m}\cdot\left[x_{2i}\cdot\left(\cos\theta_i+\cos\theta_k\right) - z_{2i}\cdot\dfrac{m\lambda}{d}\right] + 2b_{2m}\cdot y_{2i} + c_{2m} \end{cases}. \tag{25}$$

The normal vectors of the two fitted planes for the diffraction-order wavefront of the two gratings are then as shown in Eq. (26).

Optics EXPRESS

$$\begin{cases} \overrightarrow{n_{g1m}} = \left[\dfrac{a_{1m}\cdot\left(\cos\theta_i+\cos\theta_k\right)-\dfrac{m\lambda}{d}}{\left(\cos\theta_i+\cos\theta_k\right)+a_{1m}\cdot\dfrac{m\lambda}{d}}, \quad \dfrac{2b_{1m}}{\left(\cos\theta_i+\cos\theta_k\right)+a_{1m}\cdot\dfrac{m\lambda}{d}}, \quad -1 \right] \\ \overrightarrow{n_{g2m}} = \left[\dfrac{a_{2m}\cdot\left(\cos\theta_i+\cos\theta_k\right)-\dfrac{m\lambda}{d}}{\left(\cos\theta_i+\cos\theta_k\right)+a_{2m}\cdot\dfrac{m\lambda}{d}}, \quad \dfrac{2b_{2m}}{\left(\cos\theta_i+\cos\theta_k\right)+a_{2m}\cdot\dfrac{m\lambda}{d}}, \quad -1 \right] \end{cases}. \tag{26}$$

The spatial relationship between the two fitted planes for the diffraction-order wavefront of the two gratings is as shown in Eq. (27).

$$\overrightarrow{n_{g1m}}^{T} = R_x\left(\Delta\theta_x\right)\cdot R_y\left(\Delta\theta_y\right)\cdot\overrightarrow{n_{g2m}}^{T}. \tag{27}$$

And, $\Delta\theta_x$ and $\Delta\theta_y$, which correspond to the diffraction order, can be calculated using the Eq. (27). Then $\Delta\theta_z$ and Δx can be calculated by using the Eqs. (11), (13) and (25), as shown in the Eq. (28).

$$\begin{cases} \Delta\theta_z = \dfrac{\Delta\theta_x\cdot\left(\cos\theta_i+\cos\theta_k\right)+2b_{1m}}{\dfrac{m\lambda}{d}} - \dfrac{2b_{2m}\cdot\left[\left(\cos\theta_i+\cos\theta_k\right)+a_{1m}\cdot\dfrac{m\lambda}{d}\right]}{\left(\cos\theta_i+\cos\theta_k\right)\cdot\dfrac{m\lambda}{d}+a_{2m}\cdot\left(\dfrac{m\lambda}{d}\right)^2} \\ \Delta x = \dfrac{c_{2m}\cdot\left[\left(\cos\theta_i+\cos\theta_k\right)+a_{1m}\cdot\dfrac{m\lambda}{d}\right]}{\left(\cos\theta_i+\cos\theta_k\right)\cdot\dfrac{m\lambda}{d}+a_{2m}\cdot\left(\dfrac{m\lambda}{d}\right)^2} - \dfrac{c_{1m}+\Delta z\cdot\left(\cos\theta_i+\cos\theta_k\right)}{\dfrac{m\lambda}{d}} \end{cases}. \tag{28}$$

Based on the numerical matrices for the wavefront, the spatial relationships between the fitted planes for the wavefront of the two gratings can be obtained. And combining with the mathematical relationships between the grating surface and the wavefront, the mathematical model for the mosaicking errors can be established. And then the mosaicking errors can be calculated by using Eqs. (23), (27) and (28), respectively.

According to the mathematical model of the mosaicking errors, the mosaicking experiment is set up to manufacture the mosaic grating by analyzing and removing the mosaicking errors.

3. Experiments

3.1 Preparing for mosaic grating

A Zygo interferometer is used to measure the three-dimensional numerical matrix of the wavefront of the mosaic grating at a wavelength of 632.8 nm. The two gratings in the experiment are both replicas from a single master of the same generation, they have the same parameters, as following: the grating density is 79 gr/mm, the diffraction order is the −36th order, the blaze angle is −64.1373°. And the peak-to-valley (PV) values of the two gratings are 0.494 λ and 0.452 λ, where λ is the operating wavelength.

Optics EXPRESS

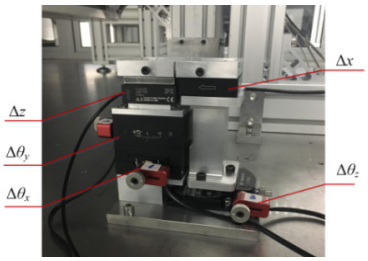

Fig. 2. Adjustment mechanisms for the mosaicking errors installed on the gratings.

To reduce the mechanical coupling, the adjustment mechanisms are installed on the two gratings according to the specific mosaicking error types, as shown in Fig. 2. The adjustment mechanisms for angle error are the actuators and the turntables, and the adjustment mechanisms for the displacement errors are the piezoelectric ceramic. The minimum step size for the actuator is 30 nm, and the gyration radii corresponding to $\Delta\theta_x$, $\Delta\theta_y$, and $\Delta\theta_z$ are 100 mm, 70 mm, and 65 mm, respectively. The piezoelectric ceramic moves in steps of 1 nm. The adjustment parameters are listed in detail in Table 1.

Table 1. Parameters of the adjustment mechanisms used for the mosaicking errors

mosaicking errors	step size /nm	radius /mm	step angle /μrad	Stoke
$\Delta\theta_x$	30	100	0.3000	12.7mm
$\Delta\theta_y$	30	70	0.4286	12.7mm
$\Delta\theta_z$	30	65	0.4615	12.7mm
Δx	1	-	-	250μm
Δz	1	-	-	250μm

Because the actuators are subject to mechanical phenomena such as idling or hysteresis, the displacements of the turntables are measured as the movement data for the angle errors, which are measured by using the inductive displacement measuring instrument during the experiments.

3.2 Mosaic gratings

The optical path of the mosaicking experiment uses the Littrow configuration.

The 0th-order optical path is as shown in Fig. 3, the light is incident perpendicular to the grating surface, where $\theta_i = \theta_k = 0°$.

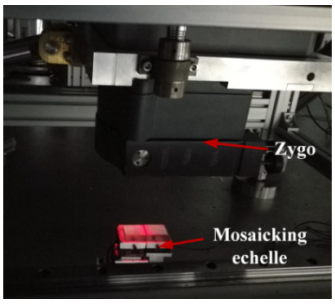

Fig. 3. Optical path for the zeroth order.

Preparations for the mosaicking experiment are as follows: First, $\Delta\theta_x$ and $\Delta\theta_y$ are adjusted coarsely to make the two far-field diffraction spots of the 0th order overlap at the center of the screen. The initial range of Δz between the two gratings is less than the Stokes value of the piezoelectric ceramic. The grating with the adjustment mechanism for $\Delta\theta_z$ is considered to be the reference grating to ensure the interference fringe is vertical and the period is suitable.

Optics EXPRESS

According to the slope, the period and the alignment of the interference fringes, the mosaic grating can be observed roughly to judge whether it is good or not. In the experiment, Δz would be removed though measuring and analyzing the zeroth-order wavefront, while $\Delta\theta_x$ and $\Delta\theta_y$ are removed preliminarily. $\Delta\theta_z$ and Δx would be removed though measuring and analyzing the diffraction-order wavefront, while $\Delta\theta_x$ and $\Delta\theta_y$ are again removed.

After the preparations, the 0th order is detected by the Zygo interferometer. And the numerical matrices for the 0th order will be measured and restored to the three-dimensional wavefront, then fitted to the planes. Figure 4(a) shows the three-dimensional map which is the fitted planes for the 0th-order wavefront of the two gratings. And Fig. 4(b) shows the corresponding intensity map, where the most of the energy of the diffracted light is concentrated in the high diffraction orders of the echelle, so the 0^{th}-order light is weak and the contrast is low.

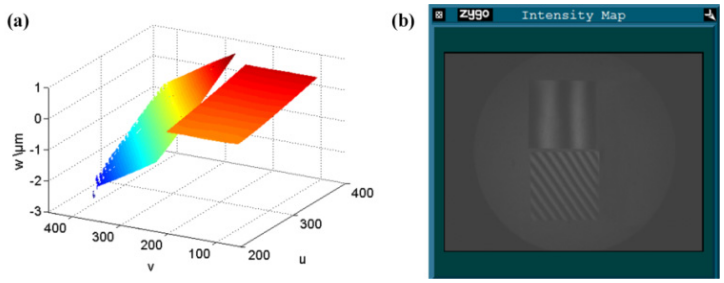

Fig. 4. Zeroth order of mosaic grating with $\Delta\theta_x$, $\Delta\theta_y$ and Δz. (a) shows the three-dimensional map, and (b) shows the intensity map.

Here, u and v are the pixels that correspond to the detector locations, w represents the wavefront data. There are angle errors between the fitted planes for the 0th-order wavefront of the two gratings, and the resulting interference fringes are inconsistent. The mosaicking errors can be calculated based on the theoretical model, as shown in Eq. (29).

$$\begin{cases} \Delta\theta_x = 88.7381\mu rad \\ \Delta\theta_y = 43.6011\mu rad \\ \Delta z = 1.0202\mu m \end{cases}. \tag{29}$$

The adjustment mechanisms are moved in accordance with Eq. (29) and Table 1. The actuator that corresponds to $\Delta\theta_x$ moves by 8.874 μm, the actuator that corresponds to $\Delta\theta_y$ moves by 3.052 μm, and the piezoelectric ceramic used to provide Δz moves by 1020 nm. The movement data are listed in Table 2.

Table 2. Movement data for the adjustment mechanisms

	$\Delta\theta_x$	$\Delta\theta_y$	Δz
values	88.7381μrad	43.6011μrad	1.0202μm
movement data	8.874μm	3.052μm	1020nm

After moving, the intensity map and the three-dimensional map are shown in Fig. 5. The two fitted planes for the 0th-order wavefront of the two gratings are in the same plane, and the interference fringes have the same period and slope, and aligned.

Optics EXPRESS

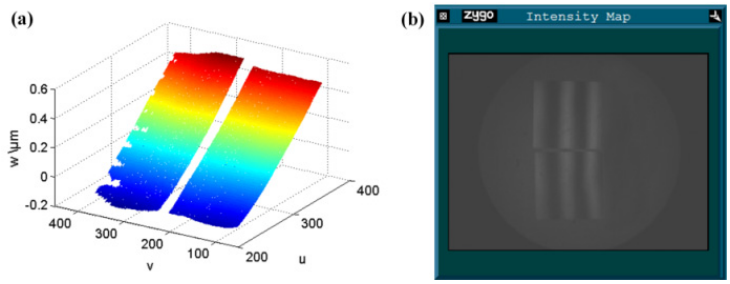

Fig. 5. Zeroth order after adjustment. (a) shows the three-dimensional map, and (b) shows the intensity map.

The residual errors can then be calculated as shown in Eq. (30).

$$\begin{cases} \Delta\theta_x = 3.0351\mu rad \\ \Delta\theta_y = 1.6051\mu rad \\ \Delta z = 8.3156nm \end{cases}. \tag{30}$$

The Zygo interferometer is then turned to the diffraction order and the mosaic grating is placed at the -36^{th} order. The optical path is as shown in Fig. 6, where $\theta_i = \theta_k = -64.1373°$.

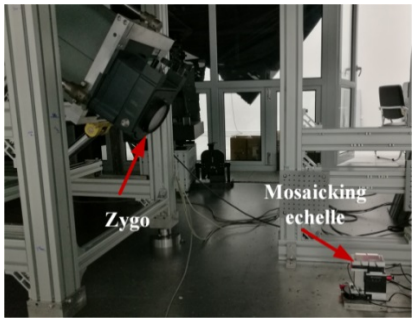

Fig. 6. Optical path for the diffraction order.

The far-field spots of the two gratings are on the same horizontal line, and separated because of $\Delta\theta_z$. And the preparation work required is described as follows: First, $\Delta\theta_z$ is adjusted coarsely to make the two far-field spots overlap at the center of the screen. The interference fringes are checked, where the grating with the adjustment mechanism for $\Delta\theta_x$ is considered to be the reference grating to ensure that the interference fringes is appropriate.

After the preparations, the -36^{th} order is detected by the Zygo interferometer. And the numerical matrices for the -36^{th} order will be measured and restored to the three-dimensional wavefront, then fitted to the planes. Figure 7(a) shows the three-dimensional map which is the fitted planes for the -36^{th}-order wavefront of the two gratings, and Fig. 7(b) shows the corresponding intensity map.

Optics EXPRESS

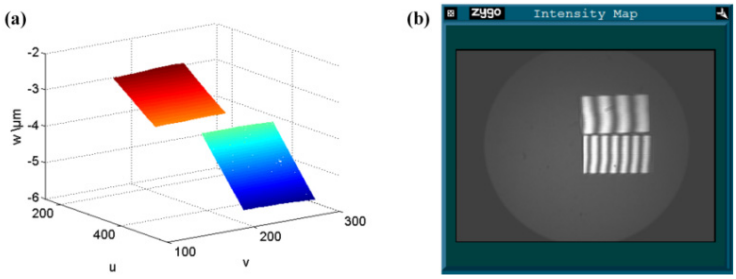

Fig. 7. The -36^{th} order of the mosaic grating with $\Delta\theta_x$, $\Delta\theta_y$, $\Delta\theta_z$, and Δz. (a) shows three-dimensional map, and (b) shows the corresponding intensity map.

The interference fringes of the two gratings are not uniform, and the two grating surfaces are thus not consistent. The mosaicking errors are then calculated based on the theoretical model, with results as shown in Eq. (31), where $\Delta z = 8.3156$ nm.

$$\begin{cases} \Delta\theta_x = 6.2789\mu rad \\ \Delta\theta_y = 20.5483\mu rad \\ \Delta\theta_z = 16.9392\mu rad \\ \Delta x = 148.5671nm \end{cases}. \tag{31}$$

The adjustment mechanisms are then moved in accordance with the Eq. (31) and Table 1. The actuator that corresponds to $\Delta\theta_x$ moves by 0.627 μm, the actuator that corresponds to $\Delta\theta_y$ moves by 1.438 μm, the actuator that corresponds to $\Delta\theta_z$ moves by 1.101 μm and the piezoelectric ceramic used to provide Δx moves by 148 nm. The movement data are listed in Table 3.

Table 3. Movement data of the adjustment mechanisms

	$\Delta\theta_x$	$\Delta\theta_y$	$\Delta\theta_z$	Δx
values	6.2789μrad	20.5483μrad	16.9392μrad	148.567nm
movement data	0.628μm	1.438μm	1.101μm	148 nm

After moving, the three-dimensional map and the intensity map are shown in Fig. 8. The two fitted planes for the 36^{th}-order wavefront of the two gratings are in the same plane, and the corresponding interference fringes have the same period and slope, and aligned.

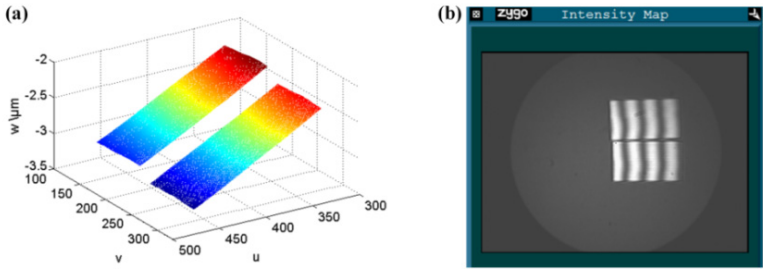

Fig. 8. The -36^{th} order after adjustment. (a) shows the three-dimensional map, and (b) shows the intensity map.

The residual errors can then be calculated, with results as shown in Eq. (32).

Optics EXPRESS

$$\begin{cases} \Delta\theta_x = 2.6308\mu rad \\ \Delta\theta_y = 0.6424\mu rad \\ \Delta\theta_z = 3.2350\mu rad \\ \Delta x = 20.4267nm \\ \Delta z = 8.3156nm \end{cases}. \quad (32)$$

As measured by the Zygo interferometer, the PV value of the mosaic grating is 0.670 λ, and point spread function (PSF) shows that the diffracted energy is concentrated at the center spot, the Strehl ratio is 0.955, as shown in Fig. 9. Figure 9 (a) is the wavefront for the mosaic grating and Fig. 9 (b) is the point spread function.

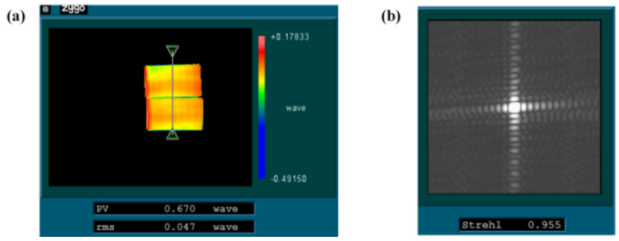

Fig. 9. Mosaic grating. (a) shows the wavefront, and (b) shows the point spread function.

4. Conclusions

A mathematical model for mosaic grating is established based on the spatial relationships between the wavefornts for the two adjacent gratings, the calculations of the mosaicking errors are given. By using the Zygo interferometer, the mosaicking experiment is set up with two gratings, where the PV values of the two gratings are 0.494λ and 0.452λ. The adjustment mechanisms are moved in accordance with the calculated mosaicking errors. We finally obtain a mosaic grating with a PV value of 0.670λ.

Funding

Ministry of Science and Technology of the People's Republic of China (2016YFF0102006, 2016YFF0103304); Jilin Province Outstanding Youth Project in China(20170520167JH); National Basic Research Program of China (2014CB049500); National Natural Science Foundation of China (NSFC) (61605204,61505204).

Acknowledgments

We thank David MacDonald, MSc, from Liwen Bianji, Edanz Editing China (www.liwenbianji.cn/ac), for editing the English text of a draft of this manuscript.

References

1. N. Bonod and J. Neauport, "Diffraction gratings: from principles to applications in high-intensity lasers," Adv. Opt. Photonics **8**(1), 156–199 (2016).
2. S. S. Vogt and D. J. Schroeder, "Introduction to the session on high resolution spectrographs," in *Instrumentation for Ground-Based Optical Astronomy* (©Springer-Verlag, 1988).
3. T. Blasiak and S. Zheleznyak, "History and construction of large mosaic diffraction gratings," Proc. SPIE **4485**, 370–377 (2002).
4. S. Mahadevan, L. Ramsey, J. Wright, M. Endl, S. Redman, C. Bender, A. Roy, S. Zonak, N. Troupe, L. Engel, S. Sigurdsson, A. Wolszczan, and B. Zhao, "The habitable zone planet finder: a proposed high-resolution NIR spectrograph for the Hobby Eberly Telescope to discover low-mass," Proc. SPIE **7735**, 77356X (2010).
5. G. De Marchi, M. B. J. te Plate, S. M. Birkmann, T. Böker, P. Ferruit, G. Giardino, P. Jakobsen, M. Sirianni, J.-C. Savignol, X. Gnata, R. Barho, M. Kosse, P. Mosner, B. Dorner, G. Cresci, F. Rosales-Ortega, M. Stuhlinger, T. Gross, and T. Leikert, "Calibrating the position of images and spectra in the NIRSpec instrument for the James Webb Space Telescope," Proc. SPIE **8150**, 81500C (2011).

Optics EXPRESS

6. J. S. Pazder, S. Roberts, R. Abraham, A. Anthony, M. Fletcher, T. Hardy, D. Loop, and S. Sun, "WFOS: a wide field optical spectrograph for the Thirty Meter Telescope," Proc. SPIE **6269**, 62691X (2006).
7. J. Qiao, A. Kalb, T. Nguyen, J. Bunkenburg, D. Canning, and J. H. Kelly, "Demonstration of large-aperture tiled-grating compressors for high-energy, petawatt-class, chirped-pulse amplification systems," Opt. Lett. **33**(15), 1684–1686 (2008).
8. J. Qiao, A. Kalb, M. J. Guardalben, G. King, D. Canning, and J. H. Kelly, "Large-aperture grating tiling by interferometry for petawatt chirped-pulse-amplification systems," Opt. Express **15**(15), 9562–9574 (2007).
9. T. J. Kessler, J. Bunkenburg, H. Huang, A. Kozlov, and D. D. Meyerhofer, "Demonstration of coherent addition of multiple gratings for high-energy chirped-pulse-amplified lasers," Opt. Lett. **29**(6), 635–637 (2004).
10. A. Cotel, C. Crotti, P. Audebert, C. Le Bris, and C. Le Blanc, "Tiled-grating compression of multiterawatt laser pulses," Opt. Lett. **32**(12), 1749–1751 (2007).
11. A. Cotel, M. Castaing, P. Pichon, and C. Le Blanc, "Phased-array grating compression for high-energy chirped pulse amplification lasers," Opt. Express **15**(5), 2742–2752 (2007).
12. Y. Ezaki, M. Tabata, M. Kihara, Y. Horiuchi, M. Endo, and T. Jitsuno, "Development of a segmented grating mount system for FIREX-1," Proceedings of the fifth International Conference on Inertial Fusion Sciences and Applications, J. Phys. Conf. Ser. **112**(3), 032027 (2008).
13. S. Montant, G. Marre, N. Blanchot, C. Rouyer, L. Videau, and C. Sauteret, "3D numerical model for a focal plane view in case of mosaic grating compressor for high energy CPA chain," Opt. Express **14**(25), 12532–12545 (2006).
14. L. Zeng and L. Li, "Method of making mosaic gratings by using a two-color heterodyne interferometer containing a reference grating," Opt. Lett. **31**(2), 152–154 (2006).
15. Y. Lu, X. Qi, X. Li, H. Yu, S. Jiang, H. Bayan, and L. Yin, "Removal of all mosaic grating errors in a single-interferometer system by a phase-difference reference window," Appl. Opt. **55**(28), 7997–8002 (2016).
16. M. Cong, X. Qi, X. Mi, H. Yu, X. Li and Y. Lu, "Influence of incident light angles on mosaic grating errors in optical path for grating replication and mosaic," Optics and Precision Engineering **25**(12), 3027–3033 (2017).
17. M. J. Guardalben, "Littrow angle method to remove alignment errors in grating pulse compressors," Appl. Opt. **47**(27), 4959–4964 (2008).
18. "Operation," in *GPI Series Interferometer Operating Manual* (© Copyright by Zygo Corporation, 2007).
19. X. Li, Bayanheshig, X. Qi, H. Yu, and Y. Tang, "Two-Dimensional Fast Fourier Transform Method of Analyzing the Influence of Plane Grating's Line Error and Surface Error on Grating's Spectral Performance," Acta Optica Sinica **32**(11), 110501 (2012).